



Published in final edited form as:

Oncogene. 2021 January ; 40(1): 112–126. doi:10.1038/s41388-020-01504-8.

MITF* is a driver oncogene and potential therapeutic target in kidney angiomyolipoma tumors through transcriptional regulation of *CYR61

Mahsa Zarei^{1,2,*}, Krinio Giannikou^{1,3,*}, Heng Du¹, Heng-Jia Liu⁴, Melissa Duarte³, Sneha Johnson², Amin H. Nassar¹, Hans R. Widlund⁵, Elizabeth P. Henske⁴, Henry W. Long³, David J. Kwiatkowski¹

¹Cancer Genetics Laboratory, Pulmonary and Critical Care Medicine, Department of Medicine, Brigham and Women's Hospital and Harvard Medical School, Boston, MA, USA

²Department of Physiology and Pharmacology, College of Veterinary Medicine and Biomedical Sciences, Texas A&M University, College Station, TX, USA

³Center for Functional Cancer Epigenetics, Department of Medical Oncology, Dana-Farber Cancer Institute and Harvard Medical School, Boston, MA, USA

⁴Pulmonary and Critical Care Medicine, Department of Medicine, Brigham and Women's Hospital and Harvard Medical School, Boston, MA, USA

⁵Department of Dermatology, Brigham and Women's Hospital, Harvard Medical School, Boston, MA, USA

Abstract

Tuberous sclerosis complex (TSC) is an autosomal dominant tumor suppressor syndrome, characterized by tumor development in multiple organs, including renal angiomyolipoma. Biallelic loss of *TSC1* or *TSC2* is a known genetic driver of angiomyolipoma development, however whether an altered transcriptional repertoire contributes to TSC-associated tumorigenesis is unknown. RNA-seq analyses showed that *MITF*A isoform (*MITF-A*) was consistently highly expressed in angiomyolipoma, immunohistochemistry showed MITF nuclear localization, and ChIP-Seq analysis showed that the *MITF-A* transcriptional start site was highly enriched with H3K27ac marks. Using the angiomyolipoma cell line 621-101, *MITF* knock out (*MITF.KO*) and *MITF-A* overexpressing (*MITF.OE*) cell lines were generated. *MITF.KO* cells showed markedly reduced growth and invasion *in vitro*, and were unable to form xenografted tumors. In contrast *MITF.OE* cells grew faster *in vitro* and as xenografted tumors compared to control cells. RNA-Seq analysis showed that both *ID2* and *CYR61* expression were increased in the *MITF.OE* cells and reduced in the *MITF.KO* cells, and luciferase assays showed this was due to transcriptional effects. Importantly, *CYR61* overexpression rescued *MITF.KO* cell growth *in vitro* and tumor growth *in*

Users may view, print, copy, and download text and data-mine the content in such documents, for the purposes of academic research, subject always to the full Conditions of use:http://www.nature.com/authors/editorial_policies/license.html#terms

Corresponding Author: David J. Kwiatkowski, M.D. Ph.D., Pulmonary and Critical Care Medicine, Department of Medicine, Brigham and Women's Hospital and Harvard Medical School, Boston, MA 02115, USA, dk@rics.bwh.harvard.edu.

*Contributed equally

Conflict of Interest: The authors declare no potential conflicts of interest.

in vivo. These findings suggest that *MITF-A* is a transcriptional oncogenic driver of angiomyolipoma tumor development, acting through regulation of *CYR61*.

Keywords

Therapeutic targets; Tuberous sclerosis complex; tumorigenesis; Angiomyolipoma; mTORC1; *MITF*; *CYR61*

Introduction

Tuberous Sclerosis Complex (TSC) is an autosomal dominant, hamartoma syndrome characterized by seizures and neurodevelopmental impairment, and tumors of the brain (subependymal giant cell astrocytoma), heart (rhabdomyomas), kidney (angiomyolipoma), and skin (angiofibroma)[1, 2]. TSC is caused by germline loss of function mutations in either *TSC1* or *TSC2*, which encode the proteins hamartin and tuberlin respectively[3, 4]. The TSC protein complex (consisting of hamartin, tuberlin, and TBC1D7) negatively regulates the activity of the mechanistic target of Rapamycin complex 1 (mTORC1) via the small GTPase RHEB [5]. mTORC1 is a serine/threonine protein kinase complex with multiple downstream targets that regulates cell growth, cell motility, protein synthesis, autophagy, transcription, and cell survival[6-8].

Angiomyolipoma and lymphangiomyomatosis (LAM) are cardinal and frequent manifestations in TSC and also occur as sporadic tumors in non-TSC individuals. Angiomyolipoma contain very few (median 4) somatic mutations in addition to bi-allelic mutation in *TSC2* (much less often *TSC1*) [9, 10]. Multiple bilateral renal angiomyolipoma occur in the majority of teenage children and adults with TSC [1, 2]. LAM occurs both at high frequency in TSC women, and as a sporadic condition in non-TSC women, and has many pathologic similarities to angiomyolipoma. Sporadic LAM has been shown to have biallelic *TSC2* inactivating mutations in the majority of cases examined in detail [11, 12]. Both angiomyolipoma and LAM show evidence of mTORC1 activation, and rapalog therapy has shown clinical benefit for both pathological entities [13, 14]. However, rapalogs typically cause a modest size reduction in angiomyolipoma, and both angiomyolipoma and LAM recur when these medications are discontinued, necessitating lifelong use. Given that, there is an unmet need to better understand the pathogenesis of these related conditions that may lead to discovery of novel therapeutic approaches.

Expression of *PMEL* (premelanosome protein, also known as SILV, gp100) has been known to be a sensitive and specific biomarker of both angiomyolipoma and LAM for over 20 years following discovery and clinical assessment of the HMB45 monoclonal antibody [15, 16]. *PMEL* is a pigment gene whose expression is regulated mainly by Microphthalmia-associated transcription factor (*MITF*)[17].

MITF is the founding member of an evolutionarily conserved transcription factor family (MiT/TFE) that also contains TFEB, TFEC, and TFE3, all of which have a conserved basic helix-loop-helix leucine-zipper structure, and can form both homo- and hetero-dimers. The *MITF* gene encodes at least 7 distinct mRNA isoforms, including several closely related M

type isoforms that have a unique transcriptional start site (TSS) that is located 200kb from the A isoform TSS[18].

In melanocytes, *MITF-M* is the predominant isoform, and *MITF* has a critical and required role in melanocyte lineage development, such that it has been termed a master transcription factor for these pigment cells [18, 19]. *MITF* target genes include those needed for melanocyte proliferation, development, differentiation, as well as genes for pigment synthesis and transport [20, 21]. *MITF* and other family members bind to E-box motifs consisting of the core hexanucleotide sequence CA[C/T]GTG[18].

In melanoma, *MITF* is often overexpressed and functions as an oncogenic transcription factor important for maintaining tumor survival and enhancing proliferation [20-22]. However, detailed analysis of *MITF* and its downstream target genes that might contribute to the growth of kidney angiomyolipoma has not been performed.

Here, we show that *MITF-A* is consistently highly expressed and functions as critical driver gene of angiomyolipoma development, promoting cell growth, migration, and invasion. We identify Cysteine-rich angiogenic inducer 61 (*CYR61*, gene symbol *CCNI*) as a novel direct target of *MITF* and find that *MITF* exerts its growth-promoting effects at least partially through upregulating *CYR61* expression. Importantly, loss of *MITF* suppressed the growth of a *TSC2*-deficient angiomyolipoma cell line in a xenograft mouse model, which was rescued by *CYR61* overexpression.

Results

***MITF-A* is relatively highly expressed in kidney angiomyolipomas**

Since previous reports have indicated that *MITF* and downstream pigment genes are expressed in angiomyolipoma and LAM [17, 27], we examined *MITF* expression in 28 kidney angiomyolipoma by RNA-Seq and compared it to datasets from The Cancer Genome Atlas (TCGA) and the Gene and Tissue Expression GTEx projects [27]. *MITF* was relatively highly expressed in angiomyolipomas, ranking 4th in comparison to 27 TCGA cancers, and was 8.4-fold ($P < 0.0001$) higher than 23 of 27 (85%) cancers, including sarcomas, another mesenchymal tumor (Figure 1A). *MITF* expression was roughly similar to that of 3 normal muscle tissues (uterus, cervix, muscle) and >6-fold higher ($P < 0.0001$) than 27 other normal tissues in the GTEx dataset (Figure 1B). The *MITF-A* isoform was the predominant isoform in kidney angiomyolipoma; no transcripts were seen beginning at the *MITF-M* promoter by inspection using IGV.

We also examined *MITF* protein expression by immunoblotting and immunohistochemical (IHC) analyses. *MITF* was detected by IHC in nearly all (6 of 7, 84%) angiomyolipomas stained, and was clearly nuclear in location in 5 of these 6 (83%) (Figures 1C-D and Supplementary Figure 1). Similarly, *MITF* was seen by IHC in LAM cells in all 3 LAM lung samples examined (Supplementary Figure 1), while minimal or no staining was seen in adjacent normal cells.

ChIP-Seq analysis identified *MITF* as a highly H3K27ac marked gene near the transcriptional start site in kidney angiomyolipoma tumors

Super-enhancers (SE) have been defined computationally as large genomic regions, typically 20-50kb, that have a high density of active chromatin marks, such as H3K27ac, and may be identified by H3K27ac Chromatin immuno-Precipitation Sequencing (ChIP-Seq). H3K27ac ChIP-Seq was performed on 8 angiomyolipomas, followed by SE analysis using ROSE (Ranking of Super Enhancer) [28, 29]. A highly marked H3K27ac region was identified beginning just upstream of the transcriptional start site (TSS) of *MITF-A* and extending downstream into intron 1 in 7 of 8 angiomyolipoma (Figure 1E, Supplementary Table 1). The median rank of *MITF* on the ROSE list of super-enhancer marked genes in these angiomyolipoma was 207, indicating that *MITF* is a highly marked gene that can be classified as a super enhancer driven TF in angiomyolipoma [28, 29].

In contrast, normal kidney had relatively light marking with H3K27ac in this region, and a pigmented melanoma cell line (SK-MEL30) had almost none at this location, while SK-MEL30 had greater H3K27ac marking near the *MITF-MTSS* (Figure 1E).

MITF promotes proliferation and anchorage-independent growth of angiomyolipoma-derived 621-101 cells

To examine the functional significance of *MITF* in angiomyolipoma disease progression in greater detail, we used a well-established human angiomyolipoma cell line 621-101 [23]. Using CRISPR/Cas9, *MITF* knock-out (*MITF.KO*) cells, 4 different clones, were generated in which marked reduction in *MITF* expression was confirmed by immunoblot and Q-RT-PCR analysis (Figure 2A and B). *MITF.KO* cells showed a striking reduction in growth in comparison to control Cas9 expressing cells (Figure 2D, 82% decrease at 96 h, $P < 0.01$). Next, we examined the effect of *MITF-A* overexpression in the 621-101 cells. The *MITF.OE* cell lines were generated using the pQCXIB plasmid containing *MITF-A* with blasticidin. Immunoblot analysis and Q-RT-PCR confirmed a marked increase in *MITF* expression (Figure 2A and C). The *MITF.OE* cells grew significantly faster (~2-fold) in comparison to control cells, and much faster than *MITF.KO* cells (Figure 2D).

We also used small interfering RNA (siRNA) oligos to inhibit the expression of *MITF* in 621-101 cells, and demonstrated a significant reduction in expression of *MITF*, with similar major effects (57%, $P < 0.01$) on growth compared with control cells (Figure 2E-G).

Consistent with these results, anchorage-independent growth assays of 621-101 cells revealed that the *MITF.KO* cells had an 82% decrease in colony number compared with control ($P < 0.01$), and that *MITF.OE* cells had an increased colony number, 1.8-fold compared to control cells ($P < 0.001$) (Figure 2H). In aggregate these data indicate that *MITF* plays a critical role in regulating the proliferation and anchorage-independent growth of the 621-101 angiomyolipoma cell line.

MITF promotes angiomyolipoma-derived 621-101 cell migration and invasion

To investigate the impact of *MITF* on angiomyolipoma cell migration, we used *MITF.KO* and *MITF.OE* cells in a transwell migration assay. *MITF.KO* cells displayed reduced

migration (70%, $P < 0.001$), while *MITF.OE* cells displayed increased migration (1.8-fold, $P < 0.001$) compared to vector control cells (Figure 2I). Similarly, *MITF.KO* cells displayed reduced invasive capacity (48%, $P < 0.01$) using a Boyden chamber invasion assay. Overexpression of *MITF* in 621-101 cells enhanced cell invasion by 2-fold compared with control ($P < 0.001$) (Figure 2J). Cells in which *MITF* expression was reduced using small interfering RNA (siRNA) oligos also showed a major reduction in both cell migration 63% ($P < 0.01$) and invasion 41% ($P < 0.05$) compared to control siRNA treated cells (Figure 2K-L). These results demonstrate that *MITF* promotes the migratory and invasive behavior of angiomyolipoma cells.

MITF is required for kidney angiomyolipoma tumor growth *in vivo*

To determine how the oncogenic properties of *MITF* impact angiomyolipoma cell growth *in vivo*, we performed xenograft experiments. Equal numbers of *MITF.KO*, *MITF.OE*, and control 621-101 cells were injected into the flanks of immunodeficient mice. The growth of control cells was slow, taking 58 days until palpable tumor nodules appeared, and such growth was significantly accelerated in mice receiving the *MITF.OE* cells (28 days until a palpable tumor nodule). Tumors did not form at all in mice receiving the *MITF.KO* cells through 70 days of observation (Figure 3A-D). Tumor volumes were measured three times per week and tumors were harvested after 70 days of tumor growth (Figure 3A). At the end of the experiment (day 70), *MITF.OE* tumor volume was increased 3.6-fold compared to controls (median values 1443 and 399 mm³); tumor weight was similarly increased 3.9-fold (Figure 3C-D). Ki-67 staining showed that the proliferation rate was markedly increased in the *MITF.OE* tumors compared to EV (Figure 3E). Q-RT-PCR analysis of tumor RNA confirmed that *MITF* mRNA levels were increased 2.2-fold that of the controls in the xenograft tumor nodules of the *MITF.OE* cells (Figure 3F). These data are clearly consistent with our *in vitro* data, and indicate that *MITF-A* overexpression enhances tumor growth in the angiomyolipoma 621-101 cells, while *MITF* loss greatly reduces their growth.

MITF knock out induces dramatic metabolic changes including accumulation of purine metabolites in 621-101 cells

To understand the effect of *MITF* Knock-out on the marked reduction in cell growth that we observed in the 621-101 cells, we analyzed the metabolome of *MITF.KO* and control (EV) 621-101 cells, using LC-MS/MS based metabolomic profiling (Supplementary Table 2). A principal component analysis (PCA) plot showed clustering of triplicate experiments, suggesting consistent differences according to *MITF* manipulation status (Figure 4A).

Multiple metabolites showed dramatic changes in levels (Supplementary Table 2, Figure 4B), as assessed by comparison of fractional TIC values in these two sets of cells (see Methods). Thirty-four (17%) of 202 metabolites showed a greater than two-fold increase in the *MITF.KO* cells compared to EV cells. Metabolite Set Enrichment Analysis (MSEA) using pathway associated metabolite sets (KEGG, Oct2019 version) revealed that these 34 upregulated metabolites were enriched for intermediates in purine metabolism, including hypoxanthine, ADP, inosine, IDP, and adenosine (Supplementary Table 2, Figure 4B). Twenty (10%) of 202 metabolites showed a greater than two-fold decrease in the *MITF.KO* cells compared to EV cells (Supplementary Table 2). These 20 down-regulated metabolites

were not enriched for any pathway associated metabolite sets by similar MSEA KEGG analysis. The most down-regulated metabolites among the 20 were UDP-N-acetylglucosamine, Carbamoyl phosphate, and 3-phospho-serine, all with a greater than four-fold reduction in levels.

RNA-Seq analysis identifies *ID2* and *CYR61* as novel candidate targets of *MITF*

In order to identify transcriptional targets of *MITF*, and the mechanism of effects of *MITF* loss and overexpression on the growth of 621-101 cells, we performed RNA-Seq. Transcripts that were differentially regulated by \log_2 fold > 1.5 and FDR < 0.05 are highlighted in red or blue (Figure 5A **right**). Comparison of *MITF.OE* cells with control 621-101 cells showed a \log_2 -fold increase > 0.58 in expression for 1452 genes, all significant at $q < 0.1$ by FDR using DESeq2 R package (Figure 5A). *MITF* had a > 8 -fold increase in expression, which was highly significant $q < 10^{-10}$ (Figure 5A **right**, Supplementary Table 3). Gene set enrichment analysis (GSEA) indicated that differentially expressed genes in the *MITF.OE* cells, compared to control cells, were enriched to a modest degree for several pathways, but none at $q < 0.1$, and hence the significance is uncertain (Supplementary Table 4). Similar analysis was performed on *MITF.KO* in comparison to control 621-101 cells, and we found a \log_2 -fold decrease > 0.58 in expression for 726 genes, all significant at $q < 0.1$ by FDR using DE-Seq2 (Figure 5A **left**, Supplementary Table 3).

We then focused on genes whose expression was both upregulated (>1.5 -fold) in the *MITF.OE* cells, and reduced (>1.5 -fold) in the *MITF.KO* cells, and also relatively highly expressed in kidney angiomyolipoma, in comparison to 27 TCGA cancers. This led to the identification of *ID2* and *CYR61* (Figure 5B and 6A). Both Q-RT-PCR experiments and immunoblotting confirmed differences in expression of both *ID2* and *CYR61* in the *MITF.OE* and *MITF.KO* cells (Figure 5C-D and Supplementary Figure 2). Similar differences were seen by Q-RT-PCR on tumor lysates from tumors formed in nude mice (Figure 5E). In summary, RNA-Seq complemented by Q-RT-PCR and western blot analyses revealed that *ID2* and *CYR61* expression are down-regulated by loss of *MITF*, and up-regulated by overexpression of *MITF*.

MITF directly binds to the promoters of *CYR61* and *ID2* in angiomyolipoma cells

We next sought to determine whether the effects of changes in *MITF* expression on *CYR61* and *ID2* expression were mediated via direct binding of *MITF* to the *CYR61* and *ID2* promoters, respectively. First, we performed *MITF*ChIP-seq on angiomyolipoma tissue samples, and observed that *MITF* bound nearby the TSS of each of these genes (Figure 5F). Second, using dual luciferase reporter constructs containing the promoter regions of each of *ID2* and *CYR61*, luciferase assays were performed. The promoter region of both *ID2* and *CYR61* had reduced luciferase expression in the *MITF.KO* angiomyolipoma cells in comparison to EV cells; and increased expression in the *MITF.OE* cells in comparison to EV cells, by 2-3-fold ($P < 0.05$) in comparison to empty vector controls (Figure 5G-H). These data suggest that both *ID2* and *CYR61* are direct targets of *MITF* in angiomyolipoma cells.

MITF expression is associated with CYR61 and ID2 in clinical specimens.

To confirm the clinical relevance of our findings, and assess the *in vivo* interaction between *MITF* and *CYR61*, and *MITF* and *ID2*, we compared their expression using our RNA-Seq dataset. There was a significant positive correlation between *MITF* expression, and *CYR61* or *ID2* expression levels in angiomyolipoma ($R^2 = 0.0735$; $P < 0.0001$; $R^2 = 0.0178$; $P < 0.0001$, respectively) (Figure 5I). In addition, *CYR61* median expression in angiomyolipoma was higher than that of 27 TCGA cancer types (6.1-fold change, $P < 0.0001$), while median *ID2* expression in angiomyolipoma was also relatively high (2.9-fold change, $P < 0.001$) compared to 25 TCGA tumors (Figure 6A-B and Supplementary Figure 3). To confirm these observations, we examined kidney angiomyolipomas by IHC. The tumors showed relatively high nuclear expression of *ID2* and high cytoplasmic expression of *CYR61*, in comparison to normal kidney by immunohistochemistry (IHC) (Figure 6C, n=3). Taken together, these data indicate that *CYR61* and *ID2* expression are each correlated with *MITF* expression in angiomyolipoma and are relatively highly expressed in this tumor.

CYR61 is a direct and functionally important target of MITF

To explore further the importance of *ID2* and *CYR61* expression in angiomyolipoma growth, and their relationship to *MITF* expression, we used CRISPR/Cas9 to knockout each gene individually in the 621-101 cells. Immunoblot analysis (Figure 6D, H) confirmed a marked reduction in *ID2* and *CYR61* expression, respectively. We found that cell migration was decreased by 65% ($P < 0.001$) (Figure 6I), cell invasion was decreased by 58% ($P < 0.05$) (Figure 6J), and proliferation was reduced by 66% ($P < 0.01$), in *CYR61*-KO cells in comparison to control (EV) (Figure 6K). In contrast, however, knock out of *ID2* in 621-101 cells had no *in vitro* measurable effect on altering migration, invasion, or proliferation (Figure 6E-G).

Next, we examined the effect of *CYR61* and *ID2* overexpression in the 621-101 cells (Figure 6D-H). Overexpression of *CYR61* increased cell migration by 1.5-fold ($P < 0.001$) (Figure 6I), invasion by 2.2-fold ($P < 0.001$) (Figure 6I) and proliferation by 1.6-fold compared with control (EV) (Figure 6K), while for *ID2.OE* cells there was no significant induction in cell migration, invasion and proliferation (Figure 6E-G). Taken together, these data indicate that *CYR61* expression enhances growth, migration, and invasion of angiomyolipoma cells.

Overexpression of CYR61 rescues the proliferation defect of MITF knockout 621-101 cells both in vitro and in vivo

Since *CYR61* is upregulated in *MITF.OE* and downregulated in *MITF.KO* cells, we examined the possibility that overexpression of *CYR61* might rescue the growth defect of the *MITF.KO* cells. Robust overexpression of *CYR61* was achieved in the *MITF.KO* +*CYR61.OE* cells (Figure 7A), and had a major effect on growth and proliferation, as compared to EV and *MITF.KO* ($P < 0.001$; $P < 0.01$, respectively) (Figure 7B-C).

Furthermore, using xenograft tumor implantation, we found that the *MITF.KO*+*CYR61.OE* cells showed a major proliferative capacity *in vivo*. *CYR61* overexpression completely rescued engraftment potential of the *MITF.KO* cells, with tumor development noted at a median of 49 days, slightly faster than 621 EV cells, for which the median had been 58 days

(Figure 7D-G). Ki67 staining showed that the proliferation rate was relatively high in the *MITF.KO+CYR61.OE* tumors intermediate to what was seen in the EV and *MITF.OE* tumors (compare Figure 7H with Figure 3E). Q-RT-PCR analysis of tumor RNA confirmed that CY61 mRNA levels were increased in the xenograft tumor nodules of the *MITF.KO+CYR61.OE* cells compared to EV tumor nodules (Figure 7I).

Taken together, these results indicate that CYR61 expression is important for angiomyolipoma cell proliferation, in this cellular model system, and may contribute to angiomyolipoma progression in patients.

Discussion

Tuberous Sclerosis Complex (TSC) is often a devastating clinical disorder in which affected children and adults are at high risk for several unusual tumors, including brain subependymal giant cell astrocytomas, cardiac rhabdomyomas, kidney and liver angiomyolipomas, facial angiofibromas, ungual fibromas, and pulmonary LAM [2]. Both angiomyolipoma and LAM also occur sporadically in patients without TSC. LAM and angiomyolipoma are leading causes of morbidity and mortality in adults with TSC. However, study of these tumors has been hindered by the availability of only a single angiomyolipoma cell line, and the lack of an authentic animal model of kidney angiomyolipoma and LAM.

Angiomyolipoma have been studied extensively to determine their mutation spectrum through exome sequencing [9, 10]. Biallelic inactivating mutations in *TSC2*, and much less commonly *TSC1*, have been seen in nearly all angiomyolipoma examined. In contrast, the somatic mutation rate excluding *TSC1/TSC2* is extremely low, with a median of 1.7 mutations per tumor. These additional mutations appear to be random occurrences reflecting the clonal origin of angiomyolipoma and without pathogenic significance. In addition, these tumors have gains or loss of a chromosome arm or chromosome in a small minority of cases, and no focal amplifications or deletions. In aggregate, these data have suggested that from a genetic point of view, the only driver of angiomyolipoma growth is loss of *TSC1/TSC2*, leading to mTORC1 activation [9, 10].

Here we pursued the hypothesis that transcription factors may also be drivers of angiomyolipoma development, alongside mTORC1 activation. We focused on *MITF* given past reports (and our own observations) that these tumors express pigment and other genes known to be regulated by *MITF* [16]. The microphthalmia family of transcription factors (*MITF*, *TFEB*, *TFE3*, and *TFEC*) is emerging as important general regulators of cancer cell survival and growth, with *MITF* functioning as a driver oncogene in melanoma, and overexpression of *MITF*, *TFE3*, and *TFEB* driven by upstream or direct gene fusion events contributing to development of several common and rare cancers [31].

Though genes regulated by *MITF* have been described in melanocytes [20, 32, 33], the functional significance of *MITF* and its roles in the pathogenesis and therapy of angiomyolipoma/LAM has not been previously explored. Here, we report that *MITF*

functions as an oncogenic transcription factor in angiomyolipoma/LAM cells by promoting cell proliferation, migration, invasion and in vivo tumor growth.

The mechanism by which *MITF* promotes angiomyolipoma/LAM growth includes upregulation of *CYR61* (CCN1), a newly identified direct target of *MITF*. *CYR61* expression is downregulated in angiomyolipoma cells with knockdown of *MITF* and upregulated in cells over-expressing *MITF*; this is the result of transcriptional regulation of *CYR61* by *MITF*. Using luciferase assays, we demonstrated that *MITF* binds to the promoter of *CYR61*. Cysteine-rich angiogenic inducer 61 (*CYR61*) belongs to the CCN (*CYR61*, CTGF and NOV) family of matricellular proteins. The role of *CYR61* in cancer progression, is highly dependent on the tumor type and the cellular context [34-36]. It has been shown that *CYR61* promotes cancer cell growth, migration and invasion in breast, gastric and ovarian cancers, gliomas and pancreatic neuroendocrine tumors [37-40]. Clinical analysis of the correlation between *CYR61* levels and tumor stage, recurrence, metastasis and overall survival has confirmed the cancer-promoting role of *CYR61* in these types of cancer [38, 39]. In other types of cancer, however, *CYR61* appears to have a tumor-suppressive role. In non-small-cell lung cancer, increased *CYR61* expression correlates with reduced tumor growth, invasiveness and progression to late-stages [41]. Of particular relevance to our findings, *CYR61* is expressed much higher in kidney angiomyolipoma in comparison to a large set of TCGA cancers. In addition, *CYR61* protein levels were high in kidney angiomyolipoma compared to normal kidney tissue by IHC. In 621-101 cells, overexpression of *CYR61* in the context of *MITF* knockdown induced cell migration, invasion and restored xenograft uptake and growth, suggesting that *CYR61* is one key downstream target contributing to the oncogenic actions of *MITF*. Interestingly *CYR61* is thought to be regulated by YAP/TAZ in other cell types [42].

Loss of *MITF* led to marked reductions in multiple metabolites through pathways and connections that are uncertain. In contrast, the increase in purine metabolites in the *MITF*KO cells seems likely to be due to a reduction in cell growth and reduced nucleotide utilization, while purine metabolism continues to be stimulated in these cells by mTORC1 signaling. It is known that mTORC1 increases expression of activating transcription factor 4 (ATF4), which regulates MTFHD2 expression leading to purine synthesis[30].

MITF is thought to play a complex role in melanoma progression, with both tumor suppressive and tumor-promoting activities. For example, high levels of *MITF* have been reported to block proliferation through upregulation of cell cycle inhibitors [43, 44]. However, *MITF* is amplified in 15% of metastatic melanomas, strongly suggesting that high expression has an oncogenic effect [45]. On the other hand, cells with low *MITF* expression are known to display invasive properties [46]. In *TSC2*-deficient kidney angiomyolipoma, *MITF* is clearly highly expressed and activated, and based on our data, functions as a tumor-growth promoting transcription factor. It is possible that differences in the function of *MITF* in angiomyolipoma compared to melanoma may be due in part to the different amino acid sequences, structures, and regulation of *MITF*-A compared to *MITF*-M.

In conclusion, reduction of *MITF* expression suppresses angiomyolipoma tumor progression by downregulating cell growth, migration, and invasion, acting at least partially through

CYR61 (*CCNI*), a direct and novel target of *MITF* in angiomyolipoma. The high expression of *MITF* and *CYR61* in angiomyolipoma patient samples, our data demonstrating effects of manipulation of levels of either, suggests they both independently and cooperatively contribute to growth of this tumor. Therefore, *MITF* and *CYR61* are potential therapeutic targets in angiomyolipoma and LAM.

Materials and Methods

Cell lines and cell culture

The 621-101 angiomyolipoma cell line [23, 24] was cultured in DMEM supplemented with 10% FBS (Gibco/Invitrogen), 1% L-glutamine (Gibco/Invitrogen), and 1% penicillin-streptomycin (Invitrogen) at 37°C in 5% humidified CO₂ incubators. CRISPR/Cas9-mediated knockouts in 621-101 cells were accomplished using guide RNAs targeting *MITF*, *CYR61* or *ID2*, fused with CRISPR/Cas9 and GFP protein. All in one lentiCRISPR vectors and CRISPR Universal Negative Control plasmid (CRISPR06-1EA) were purchased from Sigma-Aldrich. Cells were harvested after 48 h of transfection and GFP positive cells were single sorted into 96-well plates using FACS Calibur flow cytometer (BD Biosciences, East Rutherford, NJ).

The guide RNA sequences used were:

MITF-1(ttaagcgttaagcatagccat),

MITF-2(acagcaagcccaacggcag),

CYR61-1(tctcgtcaactccacctcgg),

CYR61-2(cgtaacttgaccagccga),

ID2-1(aggctcatcgggtcgtccac),

ID2-2(aacggacctcacgggactga)

A plasmid containing the *MITF-A* cDNA was available from previous studies (HW); plasmids for *CYR61* and *ID2* cDNA were purchased from GeneCopoeia and subcloned into pQCXIB-blasticidin. To make retrovirus, plasmid encoding pQCXIB (blasticidin) containing-*MITF-A*, *CYR61* or *ID2* were co-transfected with packaging (pCMV-dR8.91) and envelop (pCMV-VSVG) plasmids into 293T cells. Virus-containing supernatant was harvested, filtered with a 0.45 µm filter, and used to infect cells with 10 µg/mL polybrene. *MITF.OE*, *CYR61.OE* and *ID2.OE* cells were generated by transducing retrovirus into 621-101 cells. 4 different clones were selected in complete growth medium containing 10 µg/ml of blasticidin for 4 days, then maintained in 5 µg/ml of blasticidin. For all cell cultures experiments Mycoplasma testing (MycoAlert™ Mycoplasma Detection Kit, Lonza) was performed after each thawing and at least monthly.

Cell growth assays

Cells were plated in 96-well plates at 1×10^3 cells per well. After 5 days of incubation, cell growth was measured using Quant-iT™ PicoGreen™ dsDNA assay kit (Invitrogen)[25]. To estimate cell death, cells were trypsinized and counted after Trypan blue staining (Invitrogen) with a Hausser bright-line hemocytometer (Fisher Scientific). Low dilution plating colony formation assays were performed by plating 1,000 cells in 12-well plates. Cells were fixed with 10% formalin 9-10 days after seeding and stained with crystal violet (0.05% solution) for 30 minutes. The plates were washed extensively and imaged with a flatbed scanner. For quantification, 1 ml methanol was added to each well to extract the dye, and absorbance was measured at 540 nm using a Microplate Reader/Synergy HT BioTek plate reader.

Small RNA interference and overexpression transfections

Cells were plated at 60% confluency in 6-well plates, and transient siRNA transfections (1 μ M) were performed using Lipofectamine 3000 (Invitrogen) and Opti-MEM (Invitrogen) according to the manufacturer's protocol [25]. 48 hours after transfection, cells were treated or analyzed, as described. Small interfering RNA (siRNA) oligos were purchased from Life Technologies (si*MITF*, S8790, S8791, S8792; siCTRL, AM4635).

Immunoblot analysis

Cells were lysed using 1% Triton in TBS containing protease and phosphatase inhibitors. Tumors were lysed using 1X RIPA buffer containing protease and phosphatase inhibitors. Equal amounts of total protein were separated by electrophoresis on a 4–12% Bis-Tris gel and transferred to a PVDF membrane. Blots were blocked in 5% BSA, and then probed with antibodies against anti-*MITF* (MA5-14154, ThermoFisher Scientific), anti-*CYR61* (14479, Cell Signaling Technology), anti-*ID2* (3431, Cell Signaling Technology), and anti- α -tubulin (Sigma). Chemiluminescent (32106, Thermo Fisher Scientific) signal was captured using a Syngene G-BOX iChemi XT imager.

Anchorage-independent growth assay

The base agarose layer was prepared in 6-well culture plates by pouring 2 ml of base agarose mixture comprised of 1X DMEM, 10% FBS, and 0.5% agarose (Affymetrix). Cells were then prepared in the top agarose mixture comprised of 1X DMEM, 10% FBS, and 0.35% agarose, and poured over the solidified base agarose layer at a final seeding density of 5,000 cells/well. After solidification of the top layer, 2 ml of media were added to each well, and samples were placed in a 37°C incubator. Cells were incubated for 4 weeks, and the overlying media changed thrice weekly. At the end of the experiment, samples were rinsed twice with DPBS and fixed with 3.7% formaldehyde (Sigma-Aldrich) for 10 minutes. After two more washes with PBS, cells were stained with 0.01% crystal violet (Santa Cruz Biotechnology) for 1 hour. Pictures were taken using an Olympus SZH10 Stereo microscope (Olympus, Japan), and colonies were counted using ImageJ (<http://imagej.nih.gov/ij/>).

Migration and invasion assays

For migration assays, cells were seeded at a density of 5×10^4 cells in the upper chamber of a 6.5-mm Transwell with 8.0 μm pore polycarbonate membrane inserts (Corning) in 100 μl of serum-free DMEM for 6 h at 37 °C. Complete growth medium was placed in the bottom compartment as a chemoattractant. After incubation, non-migrated cells were wiped off from the upper surface using cotton swabs. The migrated cells on the lower surface were fixed and stained using the Differential stain kit (Newcomer Supply). Five random fields of migrated cells were imaged using a 15x objective on an Olympus FSX100 microscope; migrated cells were quantified using ImageJ analysis software.

For invasion assays, cells were seeded at a density of 2.5×10^4 cells in the upper chamber of a 6.5 mm Transwell with 8.0 μm PET membrane precoated with Matrigel (Corning) in 100 μl of serum-free DMEM for 24 h at 37°C. Invaded cells were fixed, stained, imaged, and counted, as described above.

Luciferase reporter assays

621-101 cells were seeded at 60% confluency in six well dishes, then transfected using lipofectamine 3000 (Thermo Fisher Scientific) with 2 μg of the promoter dual reporter plasmid (pCheck2–promoter *CYR61* [TSS=85580761; Upstream=1355, Downstream=201; Length=1557] or *ID2* [TSS=8681983; Upstream=1500, Downstream=176; Length=1677]), purchased from GeneCopoeia. The luciferase activity of the cultured supernatant was measured 48 h after transfection using luciferase assay reporter kit (Promega) according to the manufacturer's instructions.

Animal Studies

All experiments involving mice were blinded and conducted under the guidelines of the Brigham and Women's Hospital Institutional Animal Care and Use Committee. For all the animal studies, we have chosen to use at least five mice per group to ensure adequate power to detect difference between groups. Full details are described in the supplemental information.

ChIP-Seq and Data Analysis

ChIP-Seq was performed as previously described [26], using anti-H3K27ac (C15410196, Diagenode) or anti-*MITF* (Sigma, HPA003259). Details of ChIP-seq and data analysis are described in the supplemental information. The human tissue samples used in this study were collected on protocol 2007P000699 "Culture of LAM, AMLs, and other TSC Lesions" approved by the Partners Human Research Committee and informed consent was obtained from all subjects.

Additional methodologic details for metabolomic profiling, whole transcriptome RNA sequencing and immunohistochemistry are provided in supplemental information.

Supplementary Material

Refer to Web version on PubMed Central for supplementary material.

Acknowledgements

This work was supported by the Engles Fund for TSC and LAM; the University of Pennsylvania Orphan Disease Center in partnership with the LAM Foundation; DOD-18-1-0592 (MZ), DOD-17-1-0205 (KG) and the NIH NCI 1P01CA120964 (DJK).

References

1. Crino PB, Nathanson KL, Henske EP. The tuberous sclerosis complex. *N Engl J Med* 2006; 355: 1345–1356. [PubMed: 17005952]
2. Henske EP, Jozwiak S, Kingswood JC, Sampson JR, Thiele EA. Tuberous sclerosis complex. *Nat Rev Dis Primers* 2016; 2: 16035. [PubMed: 27226234]
3. Consortium TEctS. Identification and characterization of the tuberous sclerosis gene on chromosome 16. *Cell* 1993; 75: 1305–1315. [PubMed: 8269512]
4. van Slegtenhorst M, de Hoogt R, Hermans C, Nellist M, Janssen B, Verhoef S et al. Identification of the tuberous sclerosis gene *TSC1* on chromosome 9q34. *Science* 1997; 277: 805–808. [PubMed: 9242607]
5. Dibble CC, Elis W, Menon S, Qin W, Klekota J, Asara JM et al. TBC1D7 Is a Third Subunit of the *TSC1-TSC2* Complex Upstream of mTORC1. *Mol Cell* 2012; 47: 535–546. [PubMed: 22795129]
6. Kim DH, Sarbassov dos D, Ali SM, King JE, Latek RR, Erdjument-Bromage H et al. mTOR interacts with raptor to form a nutrient-sensitive complex that signals to the cell growth machinery. *Cell* 2002; 110: 163–175. [PubMed: 12150925]
7. Yecies JL, Manning BD. mTOR links oncogenic signaling to tumor cell metabolism. *J Mol Med* 2011; 89: 221–228. [PubMed: 21301797]
8. Zhang Y, Nicholatos J, Dreier JR, Ricoult SJ, Widenmaier SB, Hotamisligil GS et al. Coordinated regulation of protein synthesis and degradation by mTORC1. *Nature* 2014; 513: 440–443. [PubMed: 25043031]
9. Giannikou K, Malinowska IA, Pugh TJ, Yan R, Tseng YY, Oh C et al. Whole Exome Sequencing Identifies *TSC1/TSC2* Biallelic Loss as the Primary and Sufficient Driver Event for Renal Angiomyolipoma Development. *PLoS Genet* 2016; 12: e1006242. [PubMed: 27494029]
10. Martin KR, Zhou W, Bowman MJ, Shih J, Au KS, Dittenhafer-Reed KE et al. The genomic landscape of tuberous sclerosis complex. *Nat Commun* 2017; 8: 15816. [PubMed: 28643795]
11. Carsillo T, Astrinidis A, Henske EP. Mutations in the tuberous sclerosis complex gene *TSC2* are a cause of sporadic pulmonary lymphangioleiomyomatosis. *Proc Natl Acad Sci U S A* 2000; 97: 6085–6090. [PubMed: 10823953]
12. Badri KR, Gao L, Hyjek E, Schuger N, Schuger L, Qin W et al. Exonic mutations of *TSC2/TSC1* are common but not seen in all sporadic pulmonary lymphangioleiomyomatosis. *Am J Respir Crit Care Med* 2013; 187: 663–665. [PubMed: 23504366]
13. Bissler JJ, McCormack FX, Young LR, Elwing JM, Chuck G, Leonard JM et al. Sirolimus for angiomyolipoma in tuberous sclerosis complex or lymphangioleiomyomatosis. *N Engl J Med* 2008; 358: 140–151. [PubMed: 18184959]
14. McCormack FX, Inoue Y, Moss J, Singer LG, Strange C, Nakata K et al. Efficacy and Safety of Sirolimus in Lymphangioleiomyomatosis. *N Engl J Med* 2011; 364: 1595–1606. [PubMed: 21410393]
15. Bonetti F, Chiodera PL, Pea M, Martignoni G, Bosi F, Zamboni G et al. Transbronchial biopsy in lymphangioleiomyomatosis of the lung. HMB45 for diagnosis. *Am J Surg Pathol* 1993; 17: 1092–1102. [PubMed: 8214254]
16. Zavala-Pompa A, Folpe AL, Jimenez RE, Lim SD, Cohen C, Eble JN et al. Immunohistochemical study of microphthalmia transcription factor and tyrosinase in angiomyolipoma of the kidney, renal cell carcinoma, and renal and retroperitoneal sarcomas: comparative evaluation with traditional diagnostic markers. *Am J Surg Pathol* 2001; 25: 65–70. [PubMed: 11145253]
17. Hertzman Johansson C, Azimi A, Frostvik Stolt M, Shojaee S, Wiberg H, Grafstrom E et al. Association of MITF and other melanosome-related proteins with chemoresistance in melanoma tumors and cell lines. *Melanoma Res* 2013; 23: 360–365. [PubMed: 23921446]

18. Hemesath TJ, Steingrimsson E, McGill G, Hansen MJ, Vaught J, Hodgkinson CA et al. microphthalmia, a critical factor in melanocyte development, defines a discrete transcription factor family. *Genes Dev* 1994; 8: 2770–2780. [PubMed: 7958932]
19. Wellbrock C, Arozarena I. Microphthalmia-associated transcription factor in melanoma development and MAP-kinase pathway targeted therapy. *Pigment Cell Melanoma Res* 2015; 28: 390–406. [PubMed: 25818589]
20. Hoek KS, Schlegel NC, Eichhoff OM, Widmer DS, Praetorius C, Einarsson SO et al. Novel MITF targets identified using a two-step DNA microarray strategy. *Pigment Cell Melanoma Res* 2008; 21: 665–676. [PubMed: 19067971]
21. Cheli Y, Ohanna M, Ballotti R, Bertolotto C. Fifteen-year quest for microphthalmia-associated transcription factor target genes. *Pigment Cell Melanoma Res* 2010; 23: 27–40. [PubMed: 19995375]
22. Cancer Genome Atlas N. Genomic Classification of Cutaneous Melanoma. *Cell* 2015; 161: 1681–1696. [PubMed: 26091043]
23. Yu J, Astrinidis A, Howard S, Henske EP. Estradiol and tamoxifen stimulate LAM-associated angiomyolipoma cell growth and activate both genomic and nongenomic signaling pathways. *Am J Physiol Lung Cell Mol Physiol* 2004; 286: L694–700. [PubMed: 12922981]
24. Li C, Lee PS, Sun Y, Gu X, Zhang E, Guo Y et al. Estradiol and mTORC2 cooperate to enhance prostaglandin biosynthesis and tumorigenesis in *TSC2*-deficient LAM cells. *J Exp Med* 2014; 211: 15–28. [PubMed: 24395886]
25. Zarei M, Lal S, Parker SJ, Nevler A, Vaziri-Gohar A, Dukleska K et al. Posttranscriptional Upregulation of IDH1 by HuR Establishes a Powerful Survival Phenotype in Pancreatic Cancer Cells. *Cancer Res* 2017; 77: 4460–4471. [PubMed: 28652247]
26. Zarei M, Du H, Nassar AH, Yan RE, Giannikou K, Johnson SH et al. Tumors with TSC mutations are sensitive to CDK7 inhibition through NRF2 and glutathione depletion. *J Exp Med* 2019; 216: 2635–2652. [PubMed: 31506280]
27. Consortium GT. The Genotype-Tissue Expression (GTEx) project. *Nat Genet* 2013; 45: 580–585. [PubMed: 23715323]
28. Whyte WA, Orlando DA, Hnisz D, Abraham BJ, Lin CY, Kagey MH et al. Master transcription factors and mediator establish super-enhancers at key cell identity genes. *Cell* 2013; 153: 307–319. [PubMed: 23582322]
29. Loven J, Hoke HA, Lin CY, Lau A, Orlando DA, Vakoc CR et al. Selective inhibition of tumor oncogenes by disruption of super-enhancers. *Cell* 2013; 153: 320–334. [PubMed: 23582323]
30. Ben-Sahra I, Hoxhaj G, Ricoult SJH, Asara JM, Manning BD. mTORC1 induces purine synthesis through control of the mitochondrial tetrahydrofolate cycle. *Science* 2016; 351: 728–733. [PubMed: 26912861]
31. Fisher DE, Carr CS, Parent LA, Sharp PA. TFEB has DNA-binding and oligomerization properties of a unique helix-loop-helix/leucine-zipper family. *Genes Dev* 1991; 5: 2342–2352. [PubMed: 1748288]
32. Harbst K, Staaf J, Lauss M, Karlsson A, Masback A, Johansson I et al. Molecular profiling reveals low- and high-grade forms of primary melanoma. *Clin Cancer Res* 2012; 18: 4026–4036. [PubMed: 22675174]
33. Hsiao JJ, Fisher DE. The roles of microphthalmia-associated transcription factor and pigmentation in melanoma. *Arch Biochem Biophys* 2014; 563: 28–34. [PubMed: 25111671]
34. Dhar A, Ray A. The CCN family proteins in carcinogenesis. *Exp Oncol* 2010; 32: 2–9. [PubMed: 20332765]
35. Lau LF. CCN1/CYR61: the very model of a modern matricellular protein. *Cell Mol Life Sci* 2011; 68: 3149–3163. [PubMed: 21805345]
36. Mayer S, Erbes T, Timme-Bronsart S, Jaeger M, Rucker G, Kuf F et al. Clinical relevance of Cyr61 expression in patients with hormone-dependent breast cancer. *Oncol Lett* 2017; 14: 2334–2340. [PubMed: 28789451]
37. Tsai MS, Bogart DF, Castaneda JM, Li P, Lupu R. Cyr61 promotes breast tumorigenesis and cancer progression. *Oncogene* 2002; 21: 8178–8185. [PubMed: 12444554]

38. Lin MT, Zuon CY, Chang CC, Chen ST, Chen CP, Lin BR et al. Cyr61 induces gastric cancer cell motility/invasion via activation of the integrin/nuclear factor-kappaB/cyclooxygenase-2 signaling pathway. *Clin Cancer Res* 2005; 11: 5809–5820. [PubMed: 16115920]
39. Gery S, Xie D, Yin D, Gabra H, Miller C, Wang H et al. Ovarian carcinomas: CCN genes are aberrantly expressed and CCN1 promotes proliferation of these cells. *Clin Cancer Res* 2005; 11: 7243–7254. [PubMed: 16243794]
40. Huang YT, Lan Q, Ponsonnet L, Blanquet M, Christofori G, Zaric J et al. The matricellular protein CYR61 interferes with normal pancreatic islets architecture and promotes pancreatic neuroendocrine tumor progression. *Oncotarget* 2016; 7: 1663–1674. [PubMed: 26625209]
41. Tong X, O’Kelly J, Xie D, Mori A, Lemp N, McKenna R et al. Cyr61 suppresses the growth of non-small-cell lung cancer cells via the beta-catenin-c-myc-p53 pathway. *Oncogene* 2004; 23: 4847–4855. [PubMed: 15077166]
42. Zhang H, Pasolli HA, Fuchs E. Yes-associated protein (YAP) transcriptional coactivator functions in balancing growth and differentiation in skin. *Proc Natl Acad Sci U S A* 2011; 108: 2270–2275. [PubMed: 21262812]
43. Carreira S, Goodall J, Aksan I, La Rocca SA, Galibert MD, Denat L et al. Mitf cooperates with Rb1 and activates p21Cip1 expression to regulate cell cycle progression. *Nature* 2005; 433: 764–769. [PubMed: 15716956]
44. Loercher AE, Tank EM, Delston RB, Harbour JW. MITF links differentiation with cell cycle arrest in melanocytes by transcriptional activation of INK4A. *J Cell Biol* 2005; 168: 35–40. [PubMed: 15623583]
45. Garraway LA, Widlund HR, Rubin MA, Getz G, Berger AJ, Ramaswamy S et al. Integrative genomic analyses identify MITF as a lineage survival oncogene amplified in malignant melanoma. *Nature* 2005; 436: 117–122. [PubMed: 16001072]
46. Carreira S, Goodall J, Denat L, Rodriguez M, Nuciforo P, Hoek KS et al. Mitf regulation of Dial controls melanoma proliferation and invasiveness. *Genes Dev* 2006; 20: 3426–3439. [PubMed: 17182868]

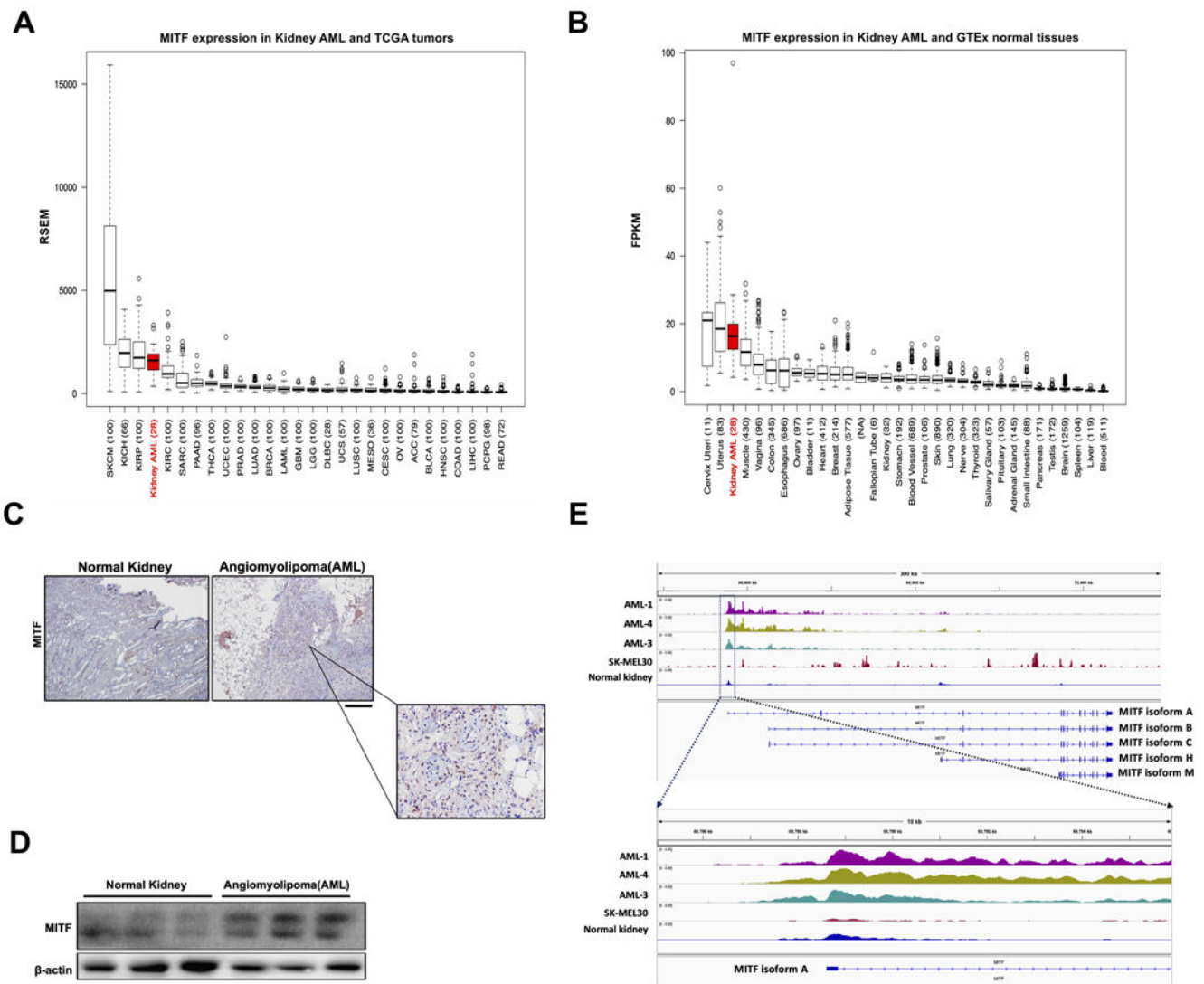


Figure 1. *MITF* is highly expressed in kidney angiomyolipomas.

(A) RNA-seq data showing *MITF* expression in 28 kidney angiomyolipomas compared to 2463 tumors of 27 different histologic types (TCGA dataset). Abbreviations for all TCGA tumor types are available here: <https://gdc.cancer.gov/resources-tcga-users/tcga-code-tables/tcga-study-abbreviations>. Gene expression is shown in RSEM values.

(B) RNA-seq data showing *MITF* expression in 28 kidney angiomyolipoma compared to GTEX human normal tissues (~8,500 samples from 30 normal tissue types, v6p release). Gene expression is shown in FPKM values.

(C) Representative IHC images show that *MITF* is expressed weakly if at all in normal kidney and highly expressed with nuclear localization in kidney angiomyolipoma. 7 kidney angiomyolipomas were examined and 6 of 7 (86%) showed *MITF* expression. Scale bar, 50 μ m.

(D) Immunoblot analysis of *MITF* in total protein lysates from 3 normal kidneys and 3 kidney angiomyolipoma tumors.

(E) H3K27ac ChIP-seq data for 3 kidney angiomyolipomas, the human melanoma SK-MEL30 cell line, and one normal kidney sample for the *MITF* locus viewed in IGV. Peaks reflecting read density for H3K27ac are seen in all three angiomyolipomas near the TSS of *MITF-A*, while few reads are seen in this region in the melanoma cell line and normal kidney. The Super-enhancer region, highly marked for H3K27ac and identified by ROSE analysis near the *MITF-A* TSS is shown at higher magnification at bottom (IGV 10kb window). Two of three angiomyolipomas shown here had *TSC2* mutations; one had a *TSC1* mutation (Supplementary Table 1).

Author Manuscript

Author Manuscript

Author Manuscript

Author Manuscript

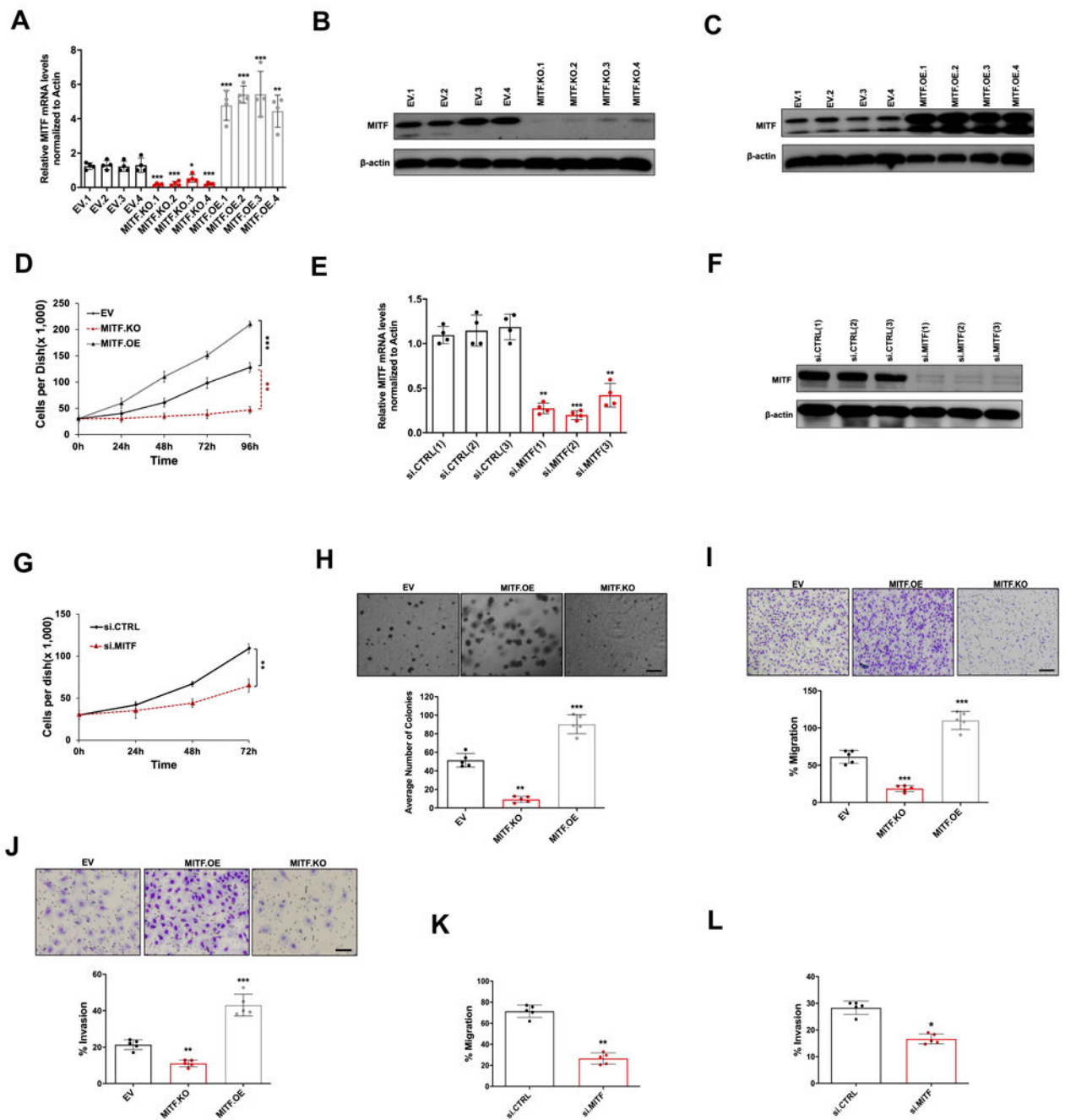


Figure 2. *MITF* regulates cell growth, proliferation, migration and invasion in 621-101 cells.

(A) Q-RT-PCR analysis of *MITF* expression after *MITF* knockout by CRISPR/Cas9 (*MITF.KO*) or overexpression of *MITF* (*MITF.OE*) compared with control (EV) in 621.101. β -actin was used as a control. Each bar represents the mean \pm SEM ($n = 4$ per group; * $p < 0.05$; ** $p < 0.01$; *** $p < 0.001$). Data for 4 separate clones is shown.

(B) Immunoblot analysis of 621-101 cells in which *MITF* has been knocked out by CRISPR/Cas9 (KO). Beta-actin serves as a loading control (3 independent experiments performed).

(C) Immunoblot analysis of 621-101 cells in which *MITF* is stably overexpressed. β -actin serves as a loading control (3 independent experiments performed). Data for 4 separate clones is shown.

(D) Cell proliferation (Trypan blue assays) of 621-101 after *MITF* knockout or overexpression compared with control (EV) for indicated time points (hours). Each data point represents the mean of 3 independent experiments \pm standard error of the mean (SEM) (** $p < 0.01$; *** $p < 0.001$).

(E) Q-RT-PCR analysis of *MITF* expression after *MITF* silencing by 3 different siRNA oligos (si.*MITF*) compared with control (si.CTRL) in 621-101 cells. Error bars represent \pm SEM of triplicate wells from a representative experiment (** $p < 0.01$; *** $p < 0.001$).

(F) Immunoblot analysis of *MITF* expression after *MITF* silencing (3 independent siRNA), along with siRNA controls in 621-101 cells. β -actin serves as a loading control (3 independent experiments performed).

(G) Cell proliferation (Trypan blue assays) of 621-101 after *MITF* silencing compared to control (si.CTRL) for indicated time points (hours). Each data point represents the mean of 3 independent experiments \pm standard error of the mean (SEM) (** $p < 0.01$).

(H) Representative images of 621-101 cells stably expressing EV, *MITF.OE* and *MITF.KO* grown in soft agar for 4 weeks. Graphs below are average number of colonies \pm SD (3 independent experiments performed, and at least 10 images per field were analyzed for each condition) (** $p < 0.01$; *** $p < 0.001$), Scale bar, 100 μ m.

(I, J) Representative images of the transwell migration assay (I) and invasion assay (J) showing decreased migration/invasion of *MITF* Knock out *MITF.KO* cells towards 10% FBS-containing growth medium; and increased migration of overexpressing *MITF.OE* cells. Error bars indicate SEM of triplicate wells from a representative experiment (3 independent experiments performed) (*** $p < 0.001$). Scale bar, 85 μ m.

(K, L) Quantification of cell migration (K) and invasion (L) by 621-101 cells with or without siRNA oligo silencing of *MITF* shows reduced migration/invasion by the si.*MITF* cells. Each data point represents the mean of 5 independent experiments \pm standard error of the mean (SEM) (** $p < 0.01$).

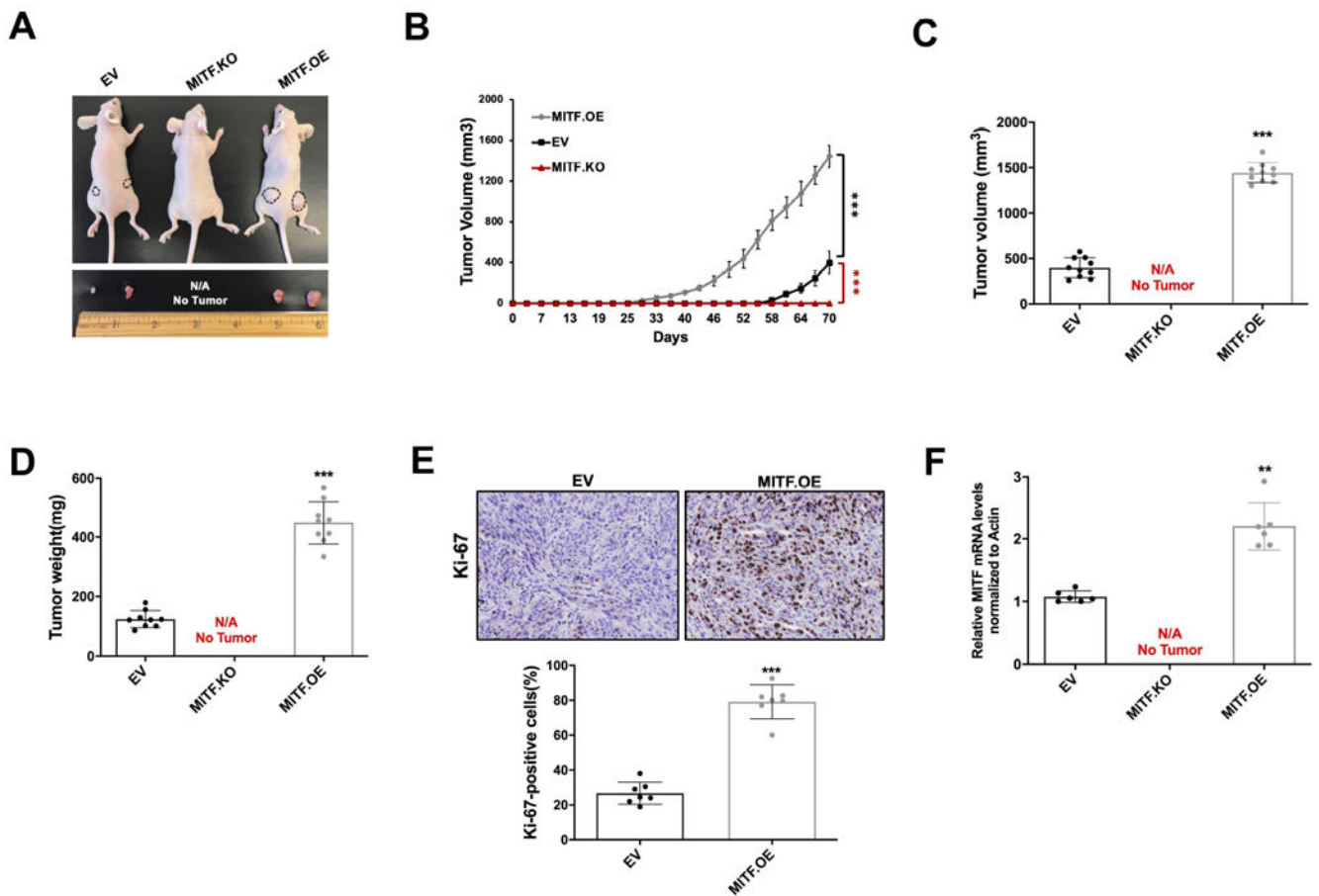


Figure 3. Effects of *MITF* knockout/overexpression on tumor xenograft development by 621-101 angiomyolipoma cells.

(A) Representative images of *in vivo* and excised xenograft tumors of 621-101 (EV, *MITF.KO* and *MITF.OE*) cells from mice, at the end of the experiment (day 70).

(B) Tumor growth curves of EV, *MITF.KO* and *MITF.OE* xenografts in nude mice are shown. Tumor size was assessed every 3 days using digital calipers. (n=5 per group, two tumors per mouse). (***) $p < 0.001$. Mean and standard deviation are shown.

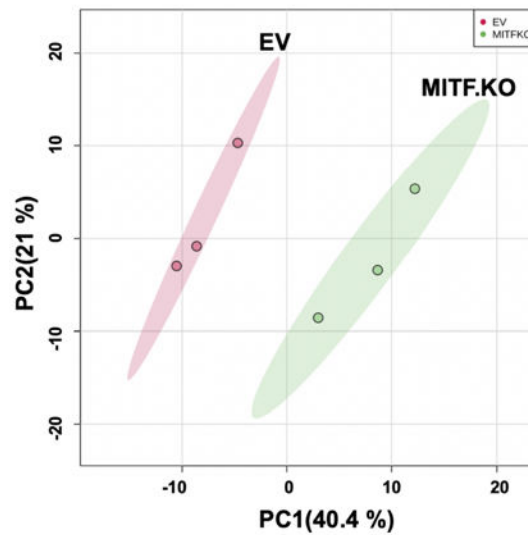
(C) Average tumor volume of 621-101 (EV, *MITF.KO* and *MITF.OE*) xenografts at the end of the experiment (day 70) (n=10 tumors per group), (***) $p < 0.001$.

(D) Average tumor weight (mg) of 621-101 (EV, *MITF.KO* and *MITF.OE*) xenograft mice in each group (n=10 per group), (***) $p < 0.001$.

(E) Tumor xenograft cell proliferation was markedly increased in mice with *MITF.OE*, in comparison to EV control, as assessed by nuclear staining by Ki-67. Quantification by counting four to six random fields per section is shown below. (***) $p < 0.001$.

(F) Q-RT-PCR analysis of *MITF* expression in 621-101 (EV and *MITF.OE*) xenografts harvested on day 70. β -actin was used as normalization control. Normalized values are shown as mean \pm SEM (n = 6 tumors per group; **) $p < 0.01$.

A



B

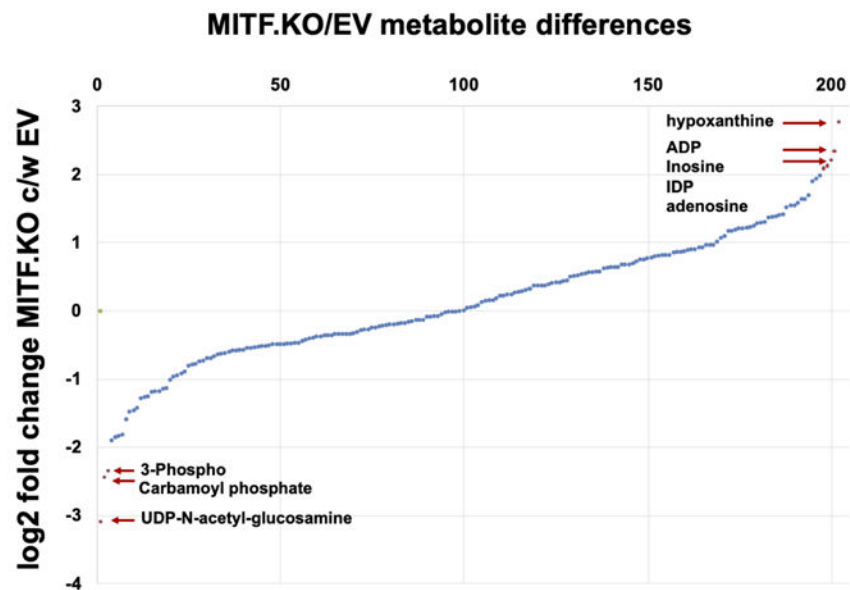


Figure 4. *MITF* inhibition induces metabolic alterations in 621-101 cells.

(A) PCA (principal component analysis) plot of metabolites generated from LC-MS/MS performed on 621-101(EV) and *MITF.KO* cells (n= 3 samples).

(B) Fold change differences in metabolites in the *MITF.KO* vs. *MITF.EV* cells are shown. Metabolites are sorted by degree of difference. The 3 metabolites with greatest reduction in the *MITF.KO* are seen at lower left, while the 5 with greatest increase are shown at upper right.

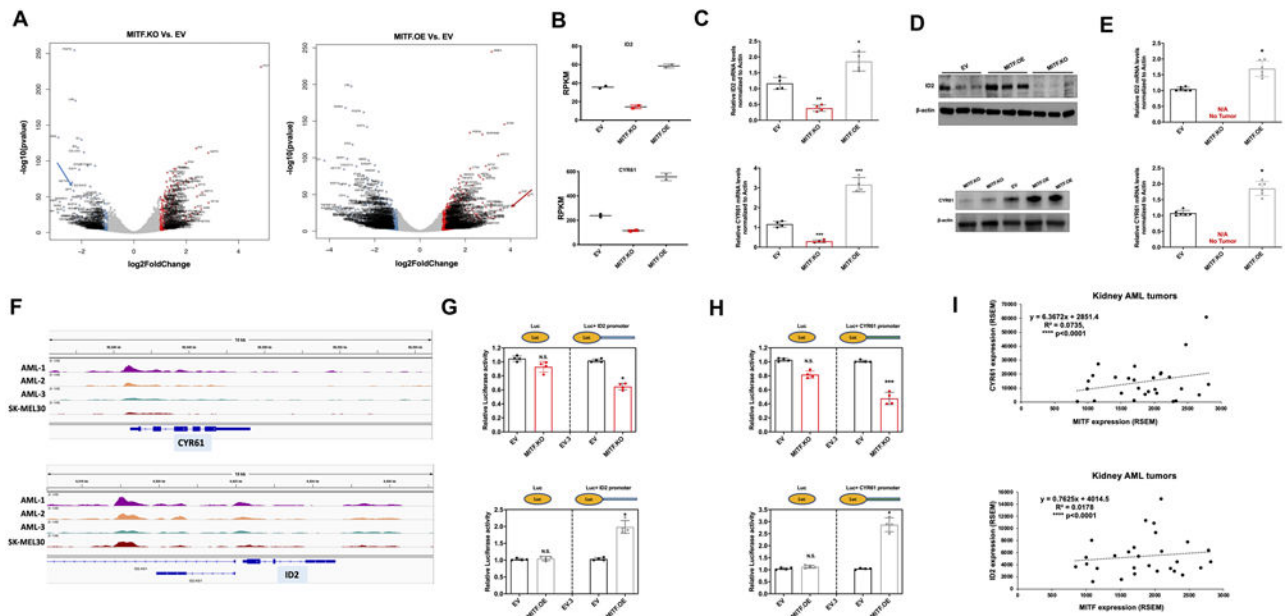


Figure 5. RNA sequencing identifies *ID2* and *CYR61* as candidate targets of *MITF*.

(A) Volcano plots of log₂fold change vs. $-\log_{10}$ (P value) of RNA-Seq data for *MITF*.KO vs. *MITF*.EV, left, and *MITF*.OE vs. *MITF*.EV, right, for 621-101 cells subject to these manipulations. Red and blue color highlights genes that showed differential expression log₂fold change > 1 (red) or < -1 (blue). *MITF* is indicated in each plot by an arrow.

(B) RNA-seq data showing *ID2* and *CYR61* expression in EV, *MITF*.KO and *MITF*.OE 621-101 cells (expression in RPKM value). (n = 2 technical replicates for each condition).

(C) Q-RT-PCR analysis of *ID2* and *CYR61* expression in EV, *MITF*.KO and *MITF*.OE 621-101 cells. Gene expression is normalized to β -actin. Each data point represents the mean \pm SEM of four independent experiments (* $p < 0.05$; *** $p < 0.001$).

(D) Immunoblot analysis of *ID2* and *CYR61* in EV, *MITF*.KO and *MITF*.OE 621-101 cells. β -actin serves as a loading control.

(E) RT-PCR analysis of *ID2* and *CYR61* expression in *MITF*.OE, *MITF*.EV, and *MITF*.KO xenografts harvested on day 70. β -actin was used as normalization control. Each bar represents the mean \pm SEM (n = 6 per group; * $p < 0.05$).

(F) IGV view of *MITF*ChIP-seq data for 3 kidney angiomyolipomas shows peaks, reflecting reads, mapping near the TSS of *CYR61* (top) and *ID2* (bottom). *MITF*ChIP-seq data from a pigmented melanoma cell line (SK-MEL30) is shown as control. Two of three angiomyolipomas shown here had *TSC2* mutations; one had a *TSC1* mutation (Supplementary Table 1).

(G, H) Dual luciferase assay of 621-101 cells with empty vector control (EV), *MITF*.KO, and *MITF* overexpression (*MITF*.OE). Cell lines were transfected with Renilla luciferase reporter constructs (G) fused with *ID2* promoter, or (H) fused with *CYR61* promoter, as well as a constitutive firefly luciferase expression construct for 24 h. Renilla luciferase activity was normalized to firefly luciferase activity, and results shown are the average of 4 experiments \pm SEM (N.S. non-significant, * $p < 0.05$, *** $p < 0.001$). The promoter regions of each gene lead to higher expression in the *MITF*.OE line, and lower in the *MITF*.KO line.

(I) Correlation analysis of *MITF* and *CYR61* expression (top panel), or *MITF* and *ID2* expression (bottom panel) in kidney angiomyolipoma (n=28) by RNA-seq data (RSEM value). Pearson correlation coefficient (R^2) and p-values are shown (**** p < 0.0001).

Author Manuscript

Author Manuscript

Author Manuscript

Author Manuscript

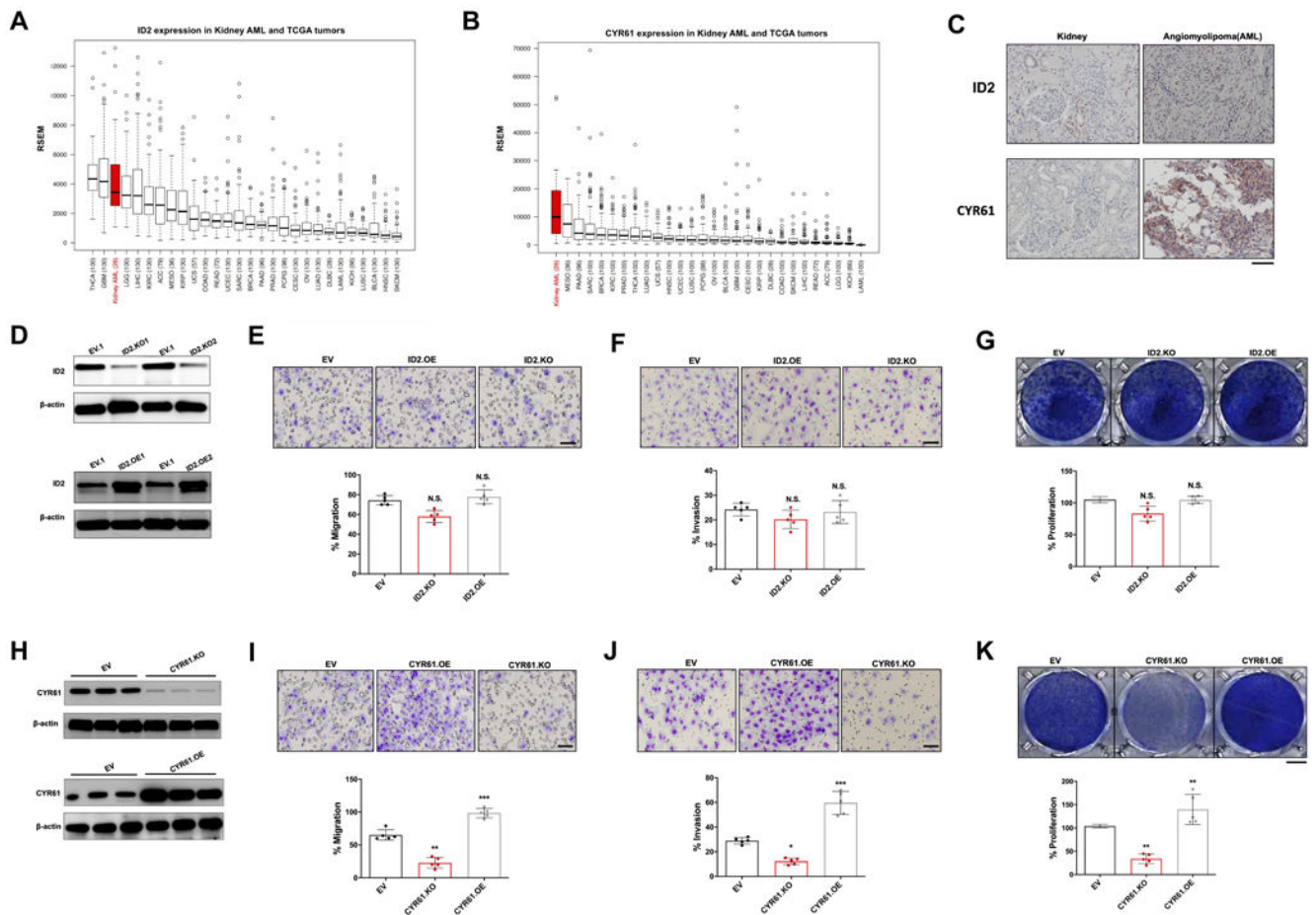


Figure 6. *ID2* and *CYR61* are expressed highly in kidney angiomyolipoma, and overexpression of *CYR61* has growth effects.

(A, B) RNA-seq data showing *ID2* (A) and *CYR61* (B) expression in 28 kidney angiomyolipomas compared to 2463 tumors of 27 different histologic types (TCGA dataset). Abbreviations for all TCGA tumor types are available here: <https://gdc.cancer.gov/resources-tcga-users/tcga-code-tables/tcga-study-abbreviations>. Gene expression is shown in RSEM values.

(C) *ID2* and *CYR61* are highly expressed in kidney angiomyolipoma by IHC.

Representative image taken from one of $n=3$ patient angiomyolipoma slides. Note nuclear localization of *ID2* and cytoplasmic localization of *CYR61*. Scale bar, 50 μ m.

(D) Immunoblot analysis of 621-101 cells in which *ID2* has been knocked out by CRISPR/Cas9 (*ID2.KO*) or stably overexpressed (*ID2.OE*). β -actin serves as a loading control. Two different clones analyzed.

(E, F) Images from a transwell assay for migration (E) and invasion (F) for the EV, *ID2.OE* and *ID2.KO* 621-101 cell lines, respectively (left to right). Quantification (%) is shown at bottom. Error bars indicate SEM of triplicate wells from a representative experiment (5 independent experiments performed for each condition) (N.S. non-significant). Scale bar, 85 μ m.

(G) Dilutional clonal growth assays show similar growth of EV, *ID2.KO*, and *ID2.OE* cells by crystal violet staining. Quantification is shown at bottom. Error bars indicate SEM of

triplicate wells from a representative experiment (3 independent experiments performed for each condition) (N.S. non-significant). Scale bar, 2 mm.

(H) Immunoblot analysis of 621-101 cells in which *CYR61* has been knocked out by CRISPR/Cas9 (*CYR61.KO*) or stably overexpressed (*CYR61.OE*). Three different clones analyzed. β -actin serves as a loading control (3 independent experiments performed).

(I, J) Representative images from a transwell assay for migration **(I)** and invasion **(J)** for the EV, *CYR61.OE* and *CYR61.KO* cell lines, respectively (left to right). Quantification is shown at bottom. Error bars indicate SEM of triplicate wells from a representative experiment (5 independent experiments performed) (** $p < 0.01$; *** $p < 0.001$). Scale bar, 85 μ m.

(K) Dilutional clonal growth assays show reduction in colony growth of *CYR61.KO* cells, and increase in colony growth *CYR61.OE* cells compared to control, crystal violet staining. Quantification is shown at bottom. Error bars indicate SEM of triplicate wells from a representative experiment (3 independent experiments performed) (** $p < 0.01$). Scale bar, 2 mm.

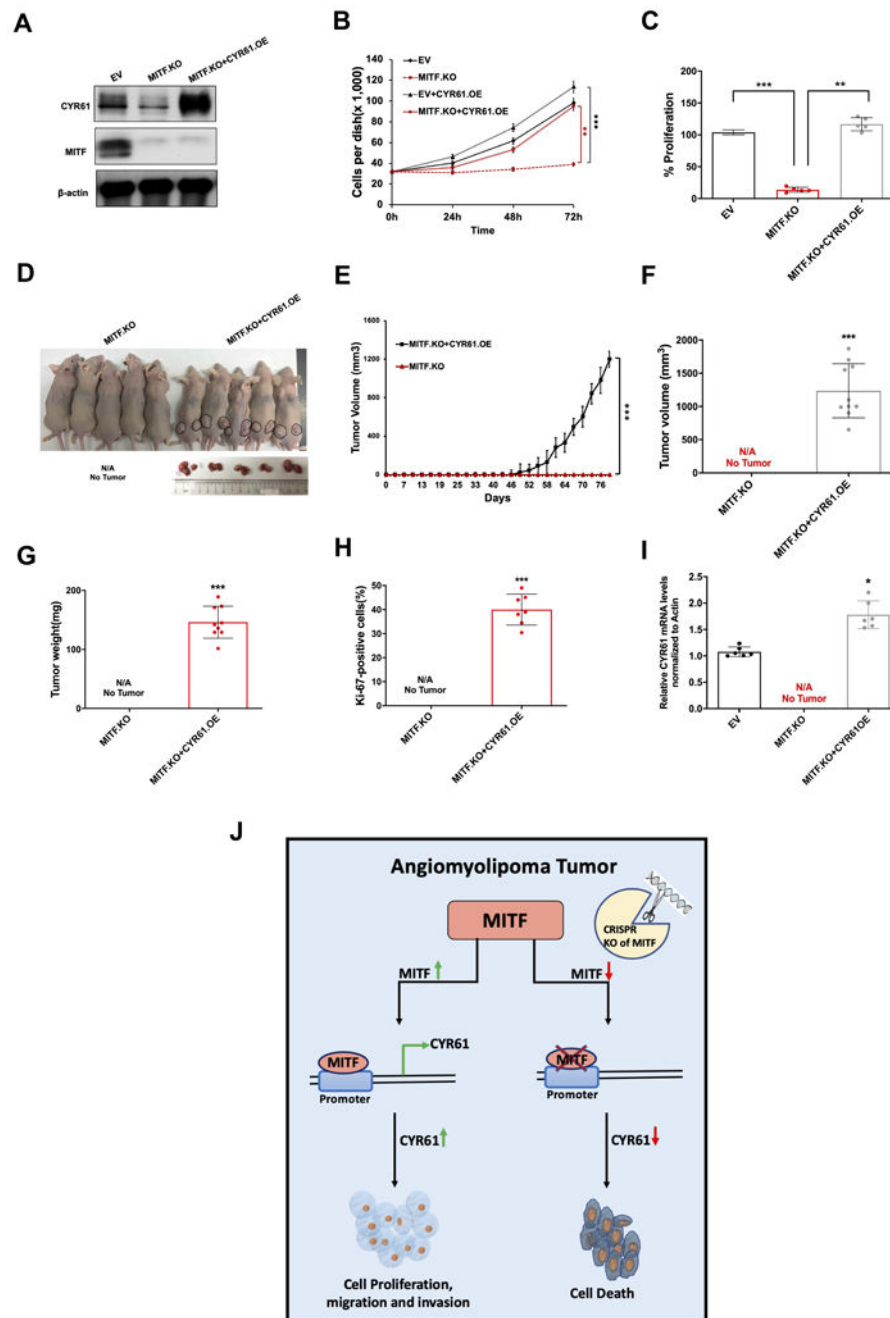


Figure 7. *CYR61* rescues *MITF*-deficient AML tumor growth *in vivo*.

(A) Immunoblot analysis of 621-101 cells in which *CYR61* overexpression was achieved in *MITF*.KO cells, yielding *MITF*.KO+*CYR61*.OE cells. β -actin serves as a loading control (2 independent experiments performed).

(B) Cell growth (Trypan blue assays) of modified 621-101 cells: EV, *MITF*.KO, EV +*CYR61*.OE, and *MITF*.KO+*CYR61*.OE. Each data point represents the mean of 3 independent experiments \pm standard error of the mean (SEM) (** $p < 0.01$; *** $p < 0.001$). *MITF*.KO+*CYR61*.OE cells show growth similar to that of EV cells.

(C) Quantification of crystal violet staining of dilutional clonal growth assays shows marked increased in colony growth of *MITF.KO*+*CYR61.OE* cells in comparison to *MITF.KO* cells. Error bars indicate SEM of triplicate wells from a representative experiment (5 independent experiments performed) (** $p < 0.01$; *** $p < 0.001$).

(D) Representative images of *in vivo* and excised xenograft tumors of 621-101-*MITF.KO*+*CYR61.OE* cells from mice, at the end of the experiment (day 80).

(E) Tumor growth curves of *MITF.KO* and *MITF.KO*+*CYR61.OE* xenografts in nude mice are shown. Tumor size was assessed every 3 days using digital calipers. (n=5 per group, two tumors per mouse). (*** $p < 0.001$).

(F) Tumor volume of 621-101(*MITF.KO* and *MITF.KO*+*CYR61.OE*) xenografts at the end of the experiment (day 80) (n=10 tumors per group), *** $p < 0.001$.

(G) Average tumor weight (mg) of 621-101 (*MITF.KO* and *MITF.KO*+*CYR61.OE*) xenograft mice in each group (n=10 per group), *** $p < 0.001$.

(H) Tumor xenograft cell proliferation was high in mice with *MITF.KO*+*CYR61.OE*, as assessed by nuclear staining using Ki-67. This was quantified by counting six random fields per section. *** $p < 0.001$. Methods identical to Figure 3E.

(I) Q-RT-PCR analysis of *CYR61* expression in 621-101 (EV, *MITF.KO* and *MITF.KO*+*CYR61.OE*) xenografts harvested on day 80. Actin was used as normalization control. Each bar represents the mean \pm SEM (n = 6 per group; ** $p < 0.05$).

(J) Diagram showing how *MITF* regulates angiomyolipoma growth and development through transcriptional regulation of *CYR61*, suggesting that these two genes form a regulatory axis, and may be an actionable therapeutic target in angiomyolipoma.